# Reactivity of Undissociated Molecular Nitric Acid at the Air−Water Interface

Josep M. Anglada,* Marilia T. C. Martins-Costa, Joseph S. Francisco,* and Manuel F. Ruiz-López*

Read Online

ACCESS | Metrics & More | Article Recommendations | SI Supporting Information

**ABSTRACT:** Recent experiments and theoretical calculations have shown that $HNO_3$ may exist in molecular form in aqueous environments, where in principle one would expect this strong acid to be completely dissociated. Much effort has been devoted to understanding this fact, which has huge environmental relevance since nitric acid is a component of acid rain and also contributes to renoxification processes in the atmosphere. Although the importance of heterogeneous processes such as oxidation and photolysis have been evidenced by experiments, most theoretical studies on hydrated molecular $HNO_3$ have focused on the acid dissociation mechanism. In the present work, we carry out calculations at various levels of theory to obtain insight into the properties of molecular nitric acid at the surface of liquid water (the air−water interface).



Through multi-nanosecond combined quantum-classical molecular dynamics simulations, we analyze the interface affinity of nitric acid and provide an order of magnitude for its lifetime with regard to acid dissociation, which is close to the value deduced using thermodynamic data in the literature (∼0.3 ns). Moreover, we study the electronic absorption spectrum and calculate the rate constant for the photolytic process $HNO_3 + h\nu \rightarrow NO_2 + OH$, leading to $2 \times 10^{-6}$ $s^{-1}$, about twice the value in the gas phase. Finally, we describe the reaction $HNO_3 + OH \rightarrow NO_3 + H_2O$ using a cluster model containing 21 water molecules with the help of high-level *ab initio* calculations. A large number of reaction paths are explored, and our study leads to the conclusion that the most favorable mechanism involves the formation of a pre-reactive complex $(HNO_3)(OH)$ from which product are obtained through a coupled proton−electron transfer mechanism that has a free-energy barrier of 6.65 kcal·$mol^{-1}$. Kinetic calculations predict a rate constant increase by ∼4 orders of magnitude relative to the gas phase, and we conclude that at the air−water interface, a lower limit for the rate constant is $k = 1.2 \times 10^{-9}$ $cm^3$·molecule$^{-1}$·$s^{-1}$. The atmospheric significance of all these results is discussed.
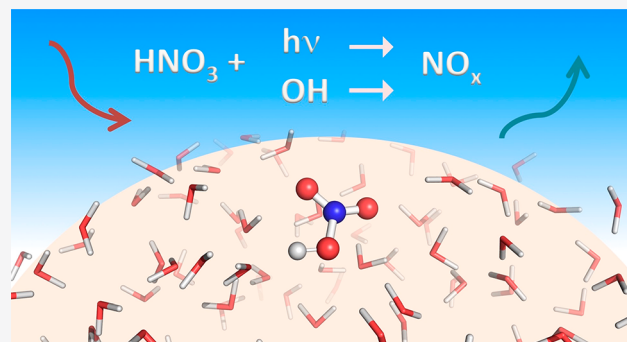
## INTRODUCTION

Rate acceleration is often observed when reactions occur at the surface of liquid water (for a recent review, see ref 1). In some cases, this phenomenon, known as "on-water catalysis",[2] can be explained simply by concentration effects, i.e., by the accumulation of hydrophobic or amphiphilic reactants at the air−water interface. In other cases, the catalytic effect derives from the unique properties of the water surface as a reaction medium, whose specific solvation effects can significantly alter the chemical behavior of the reagents. In principle, such effects can be quantified by interface-sensitive spectroscopic techniques or by computer simulations, but the physicochemical properties of the air−water interface remain largely unknown.[1] One of the most intriguing questions in this regard is the acid/ base character of the water surface and the unexpected behavior of some acidic species at the air−water interface (see, for instance, refs 3−8). The present work focuses on nitric acid, $HNO_3$, a strong acid that is completely dissociated at the usual concentrations in water solution ($pK_a = -1.3$ at 300 K) but, according to several theoretical and experimental studies,[3−5,9−14] partially undissociated at the surfaces of

various aquatic systems. These are uncommon circumstances because strong acids are expected to dissociate easily when they are hydrated by a small number of water molecules.[15] A remarkable finding of experiments and calculations is that dissociation of $HNO_3$ decreases by about 20% near the air− water interface compared with dissociation in bulk water solution,[12] although proton transfer can be strongly enhanced in the presence of electrolytes.[6,16]
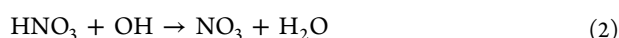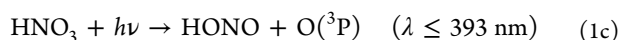
Nitric acid has great environmental relevance. Its concentration in air is typically in the range 0.048−0.795 ppb at the marine boundary, 0.18−1.77 ppb in rural or semirural areas, and 4.4−8.0 ppb in polluted areas.[17] In the gas phase, nitric acid is essentially formed by $NO_2 + OH$ and $NO + HO_2$

reactions. The aqueous phase chemistry of $HNO_3$ is very important too; owing to its high solubility (Henry's law constant $2.1 \times 10^5$ M·atm$^{-1}$), increased by dissociation to nitrate (effective Henry's law constant $3.2 \times 10^9$ M·atm$^{-1}$ at pH = 3),[18] the gas phase concentration in equilibrium with the aqueous medium is negligible.[19] In the aqueous phase, $HNO_3$ is formed by hydrolysis of $N_2O_4$, $N_2O_5$, and other oxidized species. The main reactions of molecular $HNO_3$ in the gas phase are photolysis (1) and reaction with OH (2),

$$HNO_3 + h\nu \rightarrow NO_2 + OH \quad (\lambda \leq 604 \text{ nm}) \quad (1a)$$

$$HNO_3 + h\nu \rightarrow NO_2{}^* + OH \quad (\lambda \leq 381 \text{ nm}) \quad (1b)$$

$$HNO_3 + h\nu \rightarrow HONO + O(^3P) \quad (\lambda \leq 393 \text{ nm}) \quad (1c)$$

$$HNO_3 + OH \rightarrow NO_3 + H_2O \quad (2)$$

both regenerating $NO_x$/HONO species. However, these reactions have a minor impact on the chemistry of the troposphere, even in the presence of water vapor;[20−23] the main fates of gaseous $HNO_3$ are thought to be dry and wet deposition, which contribute to "acid rain" and the acidification of soils and water. Accordingly, $HNO_3$ has traditionally been considered a sink for nitrogen oxides.

Nevertheless, in recent years, there has been increasing interest in the heterogeneous atmospheric chemistry of $HNO_3$.[14,24−26] Chemical[27] and photochemical[28−38] reactions have been shown to be enhanced when they occur on different types of solid surfaces. For instance, the photolysis rate constant of $HNO_3$ adsorbed on natural and artificial surfaces is enhanced by as much as 1−4 orders of magnitude with respect to the gas phase (see refs 33 and 39 and references cited therein). This is a fundamental result because such surface-enhanced chemistry could be a significant contributor to renoxification mechanisms, making $HNO_3$ not only a sink for nitrogen oxides but also a reservoir. Possibly, catalytic effects on reactions (1) and (2) do also occur at the surface of liquid water, but despite the potential environmental importance of such processes, especially in relation to the chemistry of microdroplets in clouds, the associated renoxification routes remain unexplored.

Many theoretical studies have been devoted to the proton transfer of $HNO_3$ to water in a variety of aqueous environments,[3−5,12,13,16,40−42] with the aim of rationalizing the available experimental data on acid dissociation. To further understand the chemistry of undissociated nitric acid "on water", in this work, we have studied the properties of the important reactions (1) and (2) at the air−water interface with the help of high-level *ab initio* calculations combined with first-principles molecular dynamics (MD) simulations. The models and methods used are briefly explained in the next section. Then, we discuss the thermodynamics of molecular nitric acid at the air−water interface, as well as the solvation effects on its main molecular properties. We briefly discuss the acid dissociation process at the interface, summarizing previous data reported in the literature and new insights obtained in our study. Finally, we report kinetic data for reactions (1) and (2), analyze the differences with respect to the chemistry of $HNO_3$ in the gas phase, and examine the atmospheric chemistry significance of our results.

## ■ METHODOLOGY

**MD Simulations.** MD simulations were carried out to get a suitable solute−solvent sampling that was subsequently used to compute properties at different ab initio levels, as described below. For this purpose, we assumed a quantum mechanics and molecular mechanics (QM/MM) potential with electrostatic embedding[43] in which $HNO_3$ is described at the B3LYP level[44] using the 6-311+G(d) basis set,[45−47] and the water solvent is described classically using a flexible TIP3P force-field.[48,49] For the solute−solvent non-electrostatic interactions, we used a Lennard-Jones potential from the OPLS force-field.[50] The choice of this combined QM/MM potential has been made based on the successful results obtained in previous studies, which showed a good balance between the different approximations for the electrostatic and non-electrostatic interaction terms.[51−59] The simulations were carried out in the NVT ensemble ($T$ = 298 K, time step 0.25 fs) using a Nosé−Hoover thermostat.[60,61] The simulation box contained $HNO_3$ and 499 $H_2O$ molecules. For the simulations at the interface, the size was (in Å) $24.662 \times 24.662 \times 130$, and we imposed periodic boundary conditions along the X and Y directions. For the simulations in bulk, the size was (in Å) $24.662 \times 24.662 \times 24.662$, and we imposed periodic boundary conditions along the X, Y, and Z directions. Our QM/MM homemade software[62] implements Gaussian 09[63] and Tinker 4.2[64] code.

As we did not impose any constraints on the system, proton transfers to classical water could have occurred. To avoid this unphysical issue, the MD trajectories were stopped when the nitric acid OH bond length became larger than a pre-defined threshold. The value $d_{OH}$ = 1.3 Å was considered the point of dissociation, based on the results of *ab initio* MD simulations.[3] After appropriate system thermalization, a single MD trajectory was carried out in bulk solution. The trajectory was stopped after 83 ps owing to the OH distance increasing beyond the pre-defined threshold, indicating a proton transfer to water. Horsetail sampling[57,58] was implemented for the simulations at the interface. In this case, there was one main (long) trajectory and many secondary (short) trajectories that complemented the sampling of the main one. The long trajectory was stopped at 267 ps to prevent unphysical proton transfer to a classical water molecule. Along this main trajectory, 75 different trajectories were launched in parallel from different starting configurations, after randomizing the atomic velocities using a Maxwell−Boltzmann distribution. Among these 75 short trajectories, nine were stopped before completion owing to fast unphysical proton transfer, while the others were carried out for ∼50 ps. The total simulation time was about 3.3 ns, which was 1−2 orders of magnitude higher than in previous studies and could provide a fairly complete general overview of $HNO_3$ solvation and dynamics at the interface.

**Electronic Spectrum.** To calculate the ultraviolet−visible light spectra, we used 581 configurations distributed along the long trajectory for $HNO_3$ at the air−water interface. The excitation energies and oscillator strengths for the lowest five singlet electronic states were calculated using a combined multireference configuration interaction (MRCI)/MM method. The MRCI calculations were carried out with a density functional theory/MRCI program (DFT/MRCI)[65] linked to the Orca program.[66] The def2-TZVPPD basis set[67,68] was employed in these calculations. All valence electrons were correlated, while 1s electrons of heavy atoms were frozen; the CI expansion was done over BHLYP orbitals. After some preliminary tests, we decided to include in the quantum-mechanical part (QM subsystem) the $HNO_3$ and the water molecules hydrogen-bonded to it (up to four water molecules); the other water molecules were treated classically as point charges. The gas phase spectrum was obtained in a similar way using 1000 configurations from a 20 ps QM simulation of isolated $HNO_3$. The cross-section was obtained through a Gaussian convolution after correcting the excitation energies and oscillator strengths to fit the experimental curve in the gas phase, as explained in the Supporting Information (SI).

**$HNO_3$ + OH Reaction Kinetics.** The potential energy surface of the $HNO_3$ + OH reaction at the air−water interface was explored using a cluster model. Specifically, we used the 21-water molecule

model that we have used in other studies of similar characteristics.[69−71] In these calculations, the stationary points were optimized and characterized, employing the B3LYP functional[44] in conjunction with the 6-311+G(2df,2p) basis set.[72,73] This functional has been chosen because (in contrast to other more recent functionals) it has proven to correctly describe the $NO_3$ radical,[44] one of the products of the reaction, which suffers from doublet instability.[74] Besides, exploratory calculations for the gas phase reaction showed that the results were not significantly improved by geometry refinement at the QCISD(T) level. However, the B3LYP approach underestimates the energy barriers for hydrogen transfer processes;[75] in order to obtain reliable relative energies, we carried out single-point energy calculations at all computed stationary points, using the DLPNO-CCSD(T) method[76] with the aug-cc-pVTZ basis set.[77,78] For comparison, the reaction mechanism and relative energies were calculated for the naked gas phase reaction and for the reactions with one and two water molecules at the DLPNO-CCSD(T)[76] and CCSD(T)[79] levels with the aug-cc-pVTZ basis set; moreover, for the naked reaction, calculations with the aug-cc-pVQZ basis set and extrapolation to the CBS (complete basis set) limit[80] were also done. The Gaussian 09[63] and Orca 4.0[66] programs were employed in these calculations. The rate constants were computed using conventional transition-state theory, considering the energies obtained at the DLPNO-CCSD(T)/aug-cc-pVTZ level and the partition functions computed at the B3LYP/6-311+G(2df,2p) level. Tunneling effects were obtained with the zero-curvature approach. The Polyrate program[81] was used for kinetic calculations.

## ■ RESULTS AND DISCUSSION

**Thermodynamics of Molecular $HNO_3$ at the Air−Water Interface.** The first important new result obtained in our study is the probability distribution describing the movements of molecular $HNO_3$ across the air−water interface. In fact, the short time-scales of previous simulations dealing with an extended interface, together with the widespread use of a biased potential fixing the position of the molecule with respect to the Gibbs-dividing surface (GDS), prevented proper characterization of such movements. The calculated density profile for the main QM/MM MD trajectory is shown in Figure 1. Remarkably, it displayed a maximum probability very
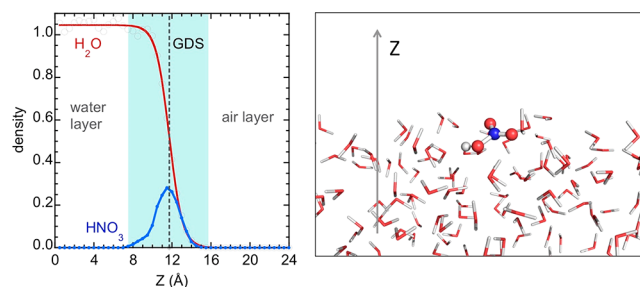


**Figure 1.** Density profiles for $HNO_3$ and water (Z = 0 corresponds to the center of the simulation box; the GDS lies at Z = 11.7 Å) and illustrative snapshot from the QM/MM simulation at the air−water interface. The density units are g·cm$^{-3}$ for water; we use arbitrary units for $HNO_3$.

small systems of atmospheric interest using a similar model.[51,52,58]

The free-energy profile for the accommodation of $HNO_3$ from gas phase to the aqueous interface and the bulk solution is not available in the literature. Obtaining this quantity is important to quantify the significance of the $HNO_3$ interfacial chemistry, but unfortunately the computational cost is exceedingly high, especially at the *ab initio* level. Here, we used parallel computing of secondary trajectories to obtain an augmented probability distribution and an estimation of the interfacial free-energy well depth (Figure S1 in the SI).[58] According to this calculation, the interface → bulk transfer process would involve not less than +1.6 kcal·mol$^{-1}$ (same reference state) suggesting interface concentration excess with an estimated interface/bulk ratio equal to 15. Using the experimental Henry's law constant for $HNO_3$, one can deduce −8.0 kcal·mol$^{-1}$ for the free energy of the gas phase → interface adsorption process. These values are subject to some uncertainties but can be considered as an approximate lower limit for the interfacial thermodynamics that were lacking in the literature.

**Interfacial Solvation Effects.** Table 1 summarizes the average of some molecular properties calculated for $HNO_3$ at

**Table 1. Values of Some $HNO_3$ Parameters in the Gas Phase (Optimized Geometry) and in Water (Averages from QM/MM MD Simulations): O−H Bond Length ($d_{OH}$, Å), O−H Bond Order ($B_{OH}$), Net Atomic Charge on H ($q_H$, e), Dipole Moment ($\mu$, D), and HOMO and LUMO Energies (eV)$^a$[84]**

| | $d_{OH}$ | $B_{OH}$ | $q_H$ | $\mu$ | HOMO | LUMO |
|---|---|---|---|---|---|---|
| gas phase | 0.973 | 0.756 | 0.477 | 2.44 | −9.5 | −2.7 |
| interface | 1.020 | 0.658 | 0.571 | 4.03 | −9.0 | −2.4 |
| bulk water | 1.020 | 0.656 | 0.572 | 4.22 | −8.9 | −2.4 |

$^a$Bond orders and atomic charges were obtained by natural bond orbital analysis.

the air−water interface. Compared with gas phase values, the OH bond was significantly elongated (+0.056 Å), in good agreement with the predictions of *ab initio* calculations in water clusters.[82,83] Besides, the molecule underwent important electronic polarization, as indicated by the significant increase in the dipole moment (+1.59 D) and the net charge on the H atom (+0.094e). Table 1 also reports the average values of the HOMO and LUMO frontier orbitals. Both were significantly destabilized at the interface. The destabilization was greater for the HOMO than for the LUMO, a result that has consequences for the photolysis rate constant because it implies that the HOMO→LUMO electronic transition will be red-shifted at the air−water interface (see the discussion below). As shown, the interfacial solvent effects were very similar to those obtained in bulk solution, except that the dipole moment seemed to be slightly smaller at the interface, possibly owing to a lower electronic polarization in this case.

To gain deeper insight into the differences between $HNO_3$ solvation at the interface and in bulk, it was worth comparing the solute−solvent radial distribution functions (RDFs) in both cases. The RDFs at the interface are shown in the left panel of Figure 2. Not surprisingly, the acidic proton formed a very strong H-bond with water. Indeed, the simulation data reveal that this H-bond was a permanent interaction along the whole trajectory. By contrast, the H-bonds formed by the O

close to the GDS, and the distribution extended approximately ±4 Å from the GDS (see SI for the method used to calculate the GDS). In other words, molecular nitric acid did not migrate to bulk in the time-scale of the simulation but, on the contrary, appeared to be quite stable at the air−water interface, confirming the findings reported by experiments. Note that the thickness of the profile was comparable to that found for other
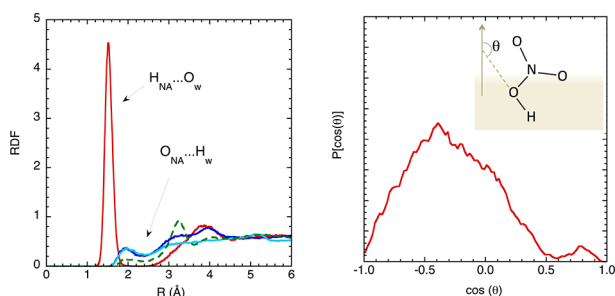
**Figure 2.** Left: radial distribution functions obtained for $HNO_3$ at the air−water interface. The curves correspond to solute−solvent hydrogen bonds in which nitric acid (NA) acts as a donor ($H_{NA}\cdots O_w$) or as an acceptor ($O_{NA}\cdots H_w$). In the latter case, the dashed line corresponds to the oxygen atom of nitric acid bonded to H, while the solid lines correspond to the other two oxygen atoms. Right: Probability distribution of the OH vector orientation.

atoms in $HNO_3$ with water protons were relatively weak, especially for the O atom in the OH group of nitric acid. Integration of the first RDF peaks led to a total average of 1.5 H-bonds between nitric acid and water. Specifically, there were 1.0, 0.2, and 0.1 H-bonds for the H, O (terminal), and O (bonded to H) atoms in $HNO_3$, respectively. For simplicity, the analysis of the RDFs in bulk is not detailed here, but the results (Figure S2 in the SI) were very similar, with a somewhat higher asymmetry for the RDFs of the terminal O atoms and a very slightly higher average number of H-bonds between nitric acid and water, which added up to 1.6. This suggests that the solvation modes of $HNO_3$ at the interface and in bulk are comparable. Previous *ab initio* simulations reported a similar conclusion when the $HNO_3$ concentration in bulk was high,[12] suggesting that an insufficient amount of water around $HNO_3$ is the driving force for a strong hydrogen bond interaction and its stabilization at the interface. Our longer simulations differ from this conclusion, however, in that the same (or very similar) solvation patterns were found for low $HNO_3$ bulk concentrations. This poses the question of the driving force for the easier dissociation in bulk. Although discussing this issue was not the aim of the present work, some comments will be made in the next section.

Figure 2 (right panel) also shows that the $HNO_3$ molecule had a preferential orientation at the air−water interface, with the OH moiety pointing toward the water layer. This was the expected result, considering the solvation pattern shown by the RDFs, and it parallels the conclusions reported previously.[12]

Finally, it is important to emphasize that the strong H-bond-donating character of nitric acid explains the observed destabilizing solvation effect on the HOMO and LUMO energies. This is the consequence of the overall negative electrostatic potential created by the H-accepting water molecule in the vicinity of the solute (due to its dipole moment orientation) and is characteristic of H-donating systems.[1,51,62]

**Acid Dissociation at the Interface.** The dissociation of $HNO_3$ at aqueous interfaces has been addressed in detail by several authors,[3−5,12,13,16,40−42] and the thermodynamics of dissociation have been shown to be strongly dependent on the location depth (i.e., the relative position with respect to the GDS).[4,5] Nevertheless, it is worth making a few comments based on the complementary results provided by our multi-nanosecond QM/MM MD simulations.

We have shown that the solvation shells of molecular $HNO_3$ at the interface and in the bulk are quite similar, despite a more favorable free energy at the interface by $\sim$1.6 kcal·mol$^{-1}$, possibly owing to a greater loss of water−water interactions in the bulk. In the dissociation process, the first step consists of the formation of a contact ion pair ($NO_3^-\cdots H$—$OH_2^+$) that precedes the diffusion of the proton to the liquid through the Grotthuss mechanism. According to first-principles MD simulations, the ion pair lies $\sim$1.8 kcal·mol$^{-1}$ above the undissociated $HNO_3$ form in bulk and $\sim$4.5 kcal·mol$^{-1}$ at the interface, where formally it does not correspond to a free-energy minimum (the values have been estimated from Figure 5 in ref 5). The combination of these data leads to the conclusion that the ion pair is thermodynamically less stable at the interface than in bulk by $\sim$1.1 kcal·mol$^{-1}$, and that dissociation is more favorable in bulk, as actually observed.

It is useful to estimate the lifetime of molecular $HNO_3$ with respect to dissociation at the interface. If one assumes the free energy required to reach the ion pair as an approximate barrier for dissociation, the lifetime is 0.32 ns (assuming a pseudo-first-order process and transition state theory; similar orders of magnitude for the dissociation energy have been reported depending on depth and interface models).[40−42] Interestingly, this lifetime is consistent with the number of pre-dissociation events that we observed in our QM/MM simulations (10 events within the 3.3 ns simulation time), confirming that the elongation of the OH bond beyond 1.3 Å is a suitable choice to characterize such events.

The energetics analysis described above is useful to explain the dissociation kinetics at the interface,[12] but understanding the whole picture would require evaluation of dissociation constants, i.e., the thermodynamics and distribution of the ions in the vicinity of the interfacial layer. Answering this question is not straightforward, even in a pure $HNO_3$ solution, and obtaining a reliable answer will require further experimental and theoretical work. It is worth remembering, however, that the nitrate anion has a low propensity for the air−water interface, according to simulations of neat nitrate solutions[85−88] and several experiments,[89,90] while the interface affinity of the hydronium ion is now broadly assumed (see the discussion in ref 1). Besides, ion distributions are influenced by the presence of other species in real systems, and this factor must be taken into account. For example, halides in sea-salt aerosols draw $NO_3^-$ anions closer to the surface.[91]

**Absorption Spectrum, Photolysis Rate Constant.** The DFT/MRCI calculations of the electronic absorption spectrum revealed a slight red-shift for the first excitation. The average excitation energies were 4.65 eV (267 nm) in the gas phase and 4.48 eV (277 nm) at the air−water interface. The shift can be explained simply by the solvation effects on the HOMO and LUMO energies, which are mainly due to the effects of the water molecule H-bonded to the nitric acid proton. The calculated cross-sections in the spectral region of atmospheric interest at 298 K are shown in Figure 3 and compared with the recommended[92] experimental values in the gas phase. The tails of the cross-sections in the 290−350 nm region, where the actinic flux rapidly increases, were relatively small and became almost negligible after 350 nm. This explains the rather low photolysis rate of gaseous nitric acid in the troposphere.[93] However, owing to the red-shift of the first excitation at the interface, the cross-section was significantly enhanced in the actinic region, suggesting an increase in the photolysis rate constant in this medium.
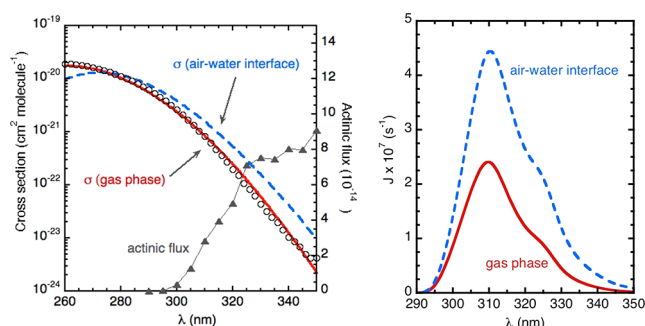
**Figure 3.** Calculated and experimental absorption cross-sections of $HNO_3$ (left) and partial photolysis rates (right). Solid and dashed lines correspond to calculations, while circles correspond to experimental values.

The rate constant for the photolysis process (1) is calculated from the expression

$$J_1 = \int_\lambda \Phi(\lambda)\sigma(\lambda)q(\lambda)\, d\lambda \tag{3}$$

where $\lambda$ is the wavelength, $\sigma$ is the absorption cross-section, $\Phi$ is the quantum yield, and $q$ is the actinic flux in the troposphere (hereafter we assume the actinic flux reported in ref 94 at the Earth's surface, noontime, and no surface Albedo). Different values have been reported for the OH quantum yield in the gas phase, which in general is close to unity in the actinic region.[92,95] Zhu et al.[96] re-examined the photolysis at 308 nm and concluded that ground-state $NO_2$ was the main product with near-unity quantum yield. Thus, for the range of wavelengths considered here, 290 nm $\leq \lambda \leq$ 350 nm, we assume that process (1a) is predominant and that $\Phi = 1$ is a good approximation.[92,95] The same quantum yield is considered for the process at the interface, assuming that solvent cage effects at the interface are not large.[97] The calculation of $J_1$ for the photolytic process (1a) is detailed in the right part of Figure 3. As shown, the main contribution to the rate constant was from light absorption at around 310 nm, both in the gas phase and at the interface. The integrated value for $J_1$ in the gas phase was $J_{1,gas} = 10^{-6}$ s$^{-1}$ using the calculated cross-section, and $9.3 \times 10^{-7}$ s$^{-1}$ using the experimental cross-section; these values are very close to other data reported in the literature ($8.2 \times 10^{-7}$ s$^{-1}$).[93] At the interface, our calculations showed an enhancement of $J$ with respect to the gas phase by a factor of 2, i.e., $J_{1,inter} = 2 \times 10^{-6}$ s$^{-1}$. This moderate increase in the photolysis rate constant of $HNO_3$ at the air–water interface contrasts with the strong increase reported for nitric acid adsorbed on a variety of surfaces.[33,39] The apparent contradiction between these data will be discussed below.

**Reaction of Nitric Acid with Hydroxyl Radical.** We analyzed the reactivity of nitric acid with a hydroxyl radical at the air–water surface by studying the process on the surface of a cluster of 21 water molecules.[69] The cluster employed in this study had a distorted pentagonal dodecahedron structure with a water molecule inside the cavity. It has eight possible anchoring sites for the reacting system, defined as oxygen atoms with a free lone-pair pointing out of the cluster and associated with a negative charge distribution (Figure S3). We thoroughly explored the different reaction paths on the cluster (see details in the SI), resulting in 16 elementary reactions for further consideration. Each elementary reaction begins with the formation of a pre-reactive (HO)($HNO_3$) complex

hydrogen-bonded to the water cluster. The reaction proceeds through a transition state that leads to the formation of $NO_3$, interacting with the augmented water cluster $(H_2O)_{22}$. As in the gas phase,[23] the transition states correspond to proton-coupled electron transfer (*pcet*) or conventional hydrogen-atom transfer (*hat*) mechanisms. The two mechanisms are illustrated in Figure 4, which displays their main electronic
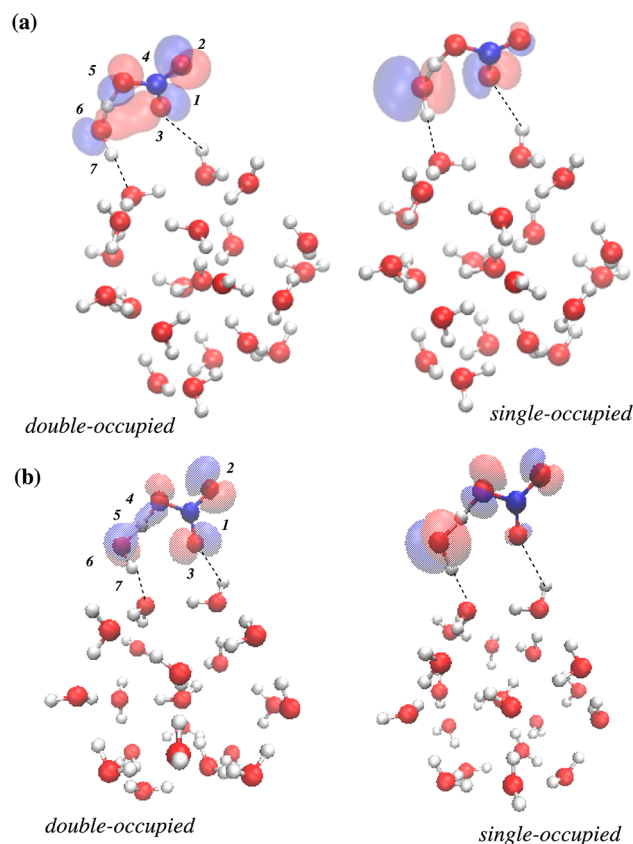


**Figure 4.** Structure of two transition states illustrating the electronic features in the (a) proton-coupled electron transfer (*pcet*) and (b) conventional hydrogen atom transfer (*hat*) reaction mechanisms. The orbital occupation is indicated.

features. In the *pcet* mechanism (Figure 4a), the radical of the hydroxyl group interacts with one of the terminal oxygen atoms of nitric acid, provoking the transfer of one electron from the $HNO_3$ moiety to the OH moiety. Simultaneously, a transfer of a proton occurs from the nitric acid to the OH moiety. The process can be described by a three-electron, two-orbital interaction between O3 and O6 (see Figure 4 for atom numbering). The *hat* mechanism (Figure 4b), instead, involves the simultaneous breaking and forming of two covalent bonds, namely, the OH bond of the nitric acid and HO bond of the hydroxyl radical. As shown, this is also a three electron, two-orbital process, but the electronic densities of the double and single natural orbitals involved entail O4 and O6, where the covalent bonds break and form. Further discussion on the characteristics of *pcet* and *hat* mechanisms for different systems can be found elsewhere.[98−106]

The calculated thermodynamic data for the 16 studied processes are detailed in the SI (Figures S4−S6 and Tables S1−S10). As shown, the relative energies of the pre-reactive complexes differed by up to 6.29 kcal·mol$^{-1}$ (Table S3). The activation free energies for the 16 processes are schematized in

Figure 5 (Table S4). The elementary reactions are denoted by the symbol "o*xtsy*", where the number *x* identifies the
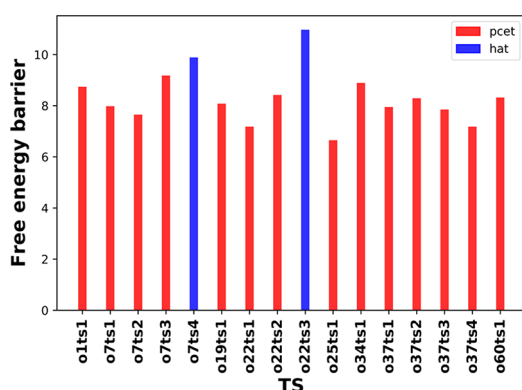


**Figure 5.** Computed free energy barrier (at 298 K) for the 16 elementary reactions investigated.



**Figure 6.** Structures for the most favorable $HNO_3$ + OH reaction path predicted on the 21-water molecules cluster.

anchoring site (oxygen atom) of the water cluster where the reaction takes place, and the number *y* identifies different elementary reactions taking place at the same site (note that *x* corresponds to the ordinal number of the oxygen atom in the Cartesian coordinates table provided in the SI).

Almost all of the elementary reactions found took place through the *pcet* mechanism (in red in Figure 5), but two of them occurred via the *hat* mechanism (in blue in Figure 5). Attempts to find other elementary reactions via *hat* mechanisms converged to *pcet* processes. As shown in Figure 5 and Table S4, the computed free-energy barriers were lower in the *pcet* mechanisms: they ranged between 6.65 and 9.18 kcal·mol$^{-1}$ (o25ts1 and o7ts3, respectively) for the elementary reactions going through the *pcet* mechanism, and between 9.89 and 10.97 kcal·mol$^{-1}$ for the reactions via the *hat* mechanism (o7ts4 and o22ts3, respectively). These differences in stability may be attributed to two main factors. The first is the effect of hydrogen bond interactions. In all transition states, there is a hydrogen bond between one oxygen atom of the water cluster and the hydrogen atom of the hydroxyl radical moiety, and a second (weaker) hydrogen bond between a dangling hydrogen atom of the cluster and one of the oxygen atoms of the $HNO_3$ moiety. In each case, there is a small charge transfer in the direction reverse to the H donation, facilitating or hampering the electron and proton transfer processes, and therefore producing a stabilizing or destabilizing effect.[23,103] The second factor is the site of the cluster where the reaction takes place. Each site is surrounded by a distinct micro-environment whose electrostatic potential affects the stability of the stationary point in a different way (see SI for full details). The structures involved in the most favorable process predicted in this study (o25ts1) are drawn in Figure 6.

The experimental kinetic constant for reaction (2) in the gas phase reported by Brown et al.[107] amounts to $k_2^{gas}$ = 1.2 × 10$^{-13}$ cm$^3$·molecule$^{-1}$·s$^{-1}$; other similar data are available in the literature.[21] Using the DLPNO-CCSD(T) thermodynamic calculations (see SI), we deduce a huge increase of this constant on the surface of the water cluster relative to the gas phase, with $k_2^{surf}/k_2^{gas} \approx 10^4$. Further analysis showed that the main effect was due to the hydrogen bonds formed with water molecules in the first solvation shell, although remaining water molecules in the cluster provided a significant long-range effect, which would conceivably be even larger if an extended
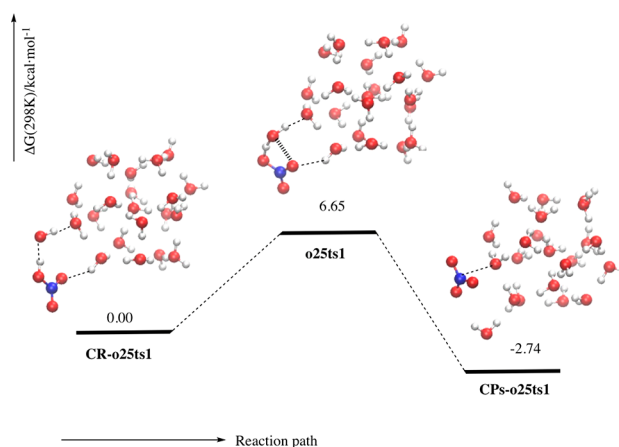
interface were considered. We conclude, therefore, that $k_2^{inter}$ ≈1.2 × 10$^{-9}$ cm$^3$·molecule$^{-1}$·s$^{-1}$ represents a lower limit for the kinetic constant of the $HNO_3$ + OH reaction at the air−water interface.

**Atmospheric Significance.** To discuss the atmospheric significance of our results, it is worth obtaining some orders of magnitude for the rates of reactions (1) and (2), $R_1$ and $R_2$, for representative concentrations of nitric acid. In the gas phase, we will take $[HNO_3]$ = 5 ppb (1.2 × 10$^{11}$ molecules·cm$^{-3}$) characteristic of polluted areas.[17] In the water droplets, we will assume pH = 4, which is representative of acid rain pH (typically lying between 4.0 and 4.6), and a nitrate concentration equal 100 $\mu$M, which is also in the range of acid rain measurements.[108] The aqueous phase to gas phase concentration ratio taken here is comparable to that predicted in photochemical box model simulations.[109] It is worth noting that inside a cloud, all the nitric acid can be considered to be dissolved in the aqueous phase and that the equilibrium gas-phase concentration is negligible.[19] Assuming the conditions above, and using the p$K_a$ of nitric acid, together with the free energy profile obtained in our work, one can estimate the interface concentration of undissociated nitric acid as 4.4 × 10$^{12}$ molecules·cm$^{-3}$, which is about 1 order of magnitude larger than $[HNO_3]$ in polluted air.

The calculated $HNO_3$ photolysis rate constant $J_1$ at the surface of liquid water is only slightly higher than in gas phase and therefore the predicted rate $R_1 = J_1[HNO_3]$ grows by 1 order of magnitude due to the concentration increase estimated above. Such small effect is not expected to influence the overall atmospheric burden of $NO_2$ since the total interfacial volume is small compared to gas phase. Interestingly, this finding differs from results reported on different artificial and natural solid surfaces.[28−39] The reason for this discrepancy is not clear. It has generally been assumed that the strong increase of the photolytic rate constant on surfaces is due to the red-shift provoked by the distorted structure of nitric acid. However, at the air−water interface, important structural changes have also been predicted, while only a moderate concomitant red-shift has been obtained. It therefore appears that interaction with water is not enough *per se* to produce a strong increase in the photolysis rate constant. As a corollary, one may deduce that photolysis on surfaces should involve effects beyond hydration, which may include the

interaction of $HNO_3$ with organic species, the formation of dimers or complexes with hydrated nitrate anions, etc.

The case of the reaction with OH leads to quite different conclusions. Using the recommended[93] annual average concentration of OH radicals in air, $[OH] = 1.16 \times 10^6$ molecules·cm$^{-3}$, and the experimental gas phase kinetic constant, we obtain a gas phase reaction rate $R_2 = k_2[HNO_3][OH] = 1.7 \times 10^4$ molecules·cm$^{-3}$·s$^{-1}$, which indicates a small contribution to renoxification of the $HNO_3$ gas phase chemistry, as outlined in the introduction. In aqueous droplets, the concentration of the OH radicals is not in equilibrium with the gas phase because due to their high reactivity, the radicals are consumed as they are formed. Indeed, $[OH]$ in aqueous droplets is in general much greater than in gas phase owing to specific OH sources.[110] Uptake from the gas phase is one of such sources but production in situ from ozone and peroxides photolysis may be up to 5 orders of magnitude larger.[53,56,111] We use here, as a lower limit, the equilibrium concentration derived from thermodynamic simulations,[112] which leads to $1.0 \times 10^{10}$ molecules·cm$^{-3}$. Consequently, the reaction rate at the interface is estimated to be $R_2 = 5.3 \times 10^{13}$ molecules·cm$^{-3}$·s$^{-1}$, which is ~9 orders of magnitude larger than the same process in air, and ~6 orders of magnitude larger than the $NO_3$ production rate from the $O_3 + NO_2$ reaction (the main $NO_3$ source in air) in polluted urban environments.[113,114] The photochemically unstable $NO_3$ radicals may diffuse and heterogeneously react with compounds adsorbed on the surface, such as isoprene or other terpenes. But due to the slightly hydrophobic character of $NO_3$,[115] a fraction of the formed radicals should be released to the gas phase and contribute to renoxification mechanisms. In principle, reactions (1) and (2) can also occur in bulk solution, but their contribution to renoxification is expected to be less important than for interfacial chemistry. The concentrations of undissociated nitric acid and OH[112] are much lower in that case, and the small amounts of the formed nitrate radicals, not likely to escape to the air, should react quickly in the aqueous phase[116] before wet deposition.

## CONCLUSIONS

In water droplets, most of nitric acid is in the form of nitrate, but a fraction of undissociated $HNO_3$ exists at the surface. Previous studies have reported that surficial dissociation decreases by about 20% compared with bulk in neat water,[12] but the atmospheric significance of the resulting concentration is still under debate. The water content of clouds, the size of droplets, their chemical composition, and the thermodynamic conditions are certainly important parameters that need to be considered.

In this work, we have studied the photolysis and the reaction with OH of undissociated nitric acid at the air−water interface with the help of high-level theoretical methods. The main results are as follows: (1) $HNO_3$ appears to be quite stable at the interface; we predict a free energy of adsorption of ~ −8.0 kcal·mol$^{-1}$ (gas phase → interface process) and an interface preference with respect to bulk of ~1.6 kcal·mol$^{-1}$. (2) The solvation pattern and the solvation effect of $HNO_3$ properties at the interface are not very different compared with solvation in bulk. (3) The reduced acid dissociation at the interface is most probably due to the lower stability of the ion pair formed in the early steps of the process. (4) The photolysis rate constant at the interface in the actinic region is larger than that in the gas phase by a factor of 2, which is smaller than the

increase reported on several solid surfaces, suggesting the existence of effects other than hydration in the latter case. (5) The redox reaction with OH is hugely enhanced at the interface with respect to gas phase due to significant reaction rate increase and large reactant accumulation, therefore this process may be a significant contributor to renoxification processes in the troposphere.

The more general conclusion of this study is that the chemistry of undissociated strong acids in aqueous environments, which represents an unusual situation in chemistry, has important specificities that should be investigated in greater detail. Indeed, fundamental processes as important as acid−base reactions at the surface of water are still poorly understood,[1] and unraveling the associated mechanisms is probably one of the most appealing chemical problems to address in the field of aqueous interfaces.

## ■ ASSOCIATED CONTENT

### ⓈⒾ Supporting Information

The Supporting Information is available free of charge at https://pubs.acs.org/doi/10.1021/jacs.0c11841.

　　Details on calculations, $HNO_3$ free energy profile, radial distribution functions in bulk water, Tables S1−S6, Figures S1−S10, atomic coordinates for the $HNO_3$ + OH reaction on the 21-water molecules cluster (PDF)

## ■ AUTHOR INFORMATION

### Corresponding Authors

**Josep M. Anglada** − *Departament de Química Biològica, Institut de Química Avançada de Catalunya (IQAC − CSIC), E-08034 Barcelona, Spain;* ⊙ orcid.org/0000-0003-4526-3624; Email: anglada@iqac.csic.es

**Joseph S. Francisco** − *Department of Earth and Environmental Science and Department of Chemistry, University of Pennsylvania, Philadelphia, Pennsylvania 19104-6316, United States;* ⊙ orcid.org/0000-0002-5461-1486; Email: frjoseph@sas.upenn.edu

**Manuel F. Ruiz-López** − *Laboratoire de Physique et Chimie Théoriques, UMR CNRS 7019, University of Lorraine, 54506 Vandoeuvre-lès-Nancy, France;* ⊙ orcid.org/0000-0002-2784-6319; Email: manuel.ruiz@univ-lorraine.fr

### Author

**Marilia T. C. Martins-Costa** − *Laboratoire de Physique et Chimie Théoriques, UMR CNRS 7019, University of Lorraine, 54506 Vandoeuvre-lès-Nancy, France;* ⊙ orcid.org/0000-0003-4957-2248

Complete contact information is available at:
https://pubs.acs.org/10.1021/jacs.0c11841

### Notes

The authors declare no competing financial interest.

## ■ REFERENCES

(1) Ruiz-Lopez, M. F.; Francisco, J. S.; Martins-Costa, M. T. C.; Anglada, J. M. Molecular reactions at aqueous interfaces. *Nat. Rev. Chem.* **2020**, *4*, 459−475.

(2) Narayan, S.; Muldoon, J.; Finn, M. G.; Fokin, V. V.; Kolb, H. C.; Sharpless, K. B. On water: Unique reactivity of organic compounds in aqueous suspension. *Angew. Chem., Int. Ed.* **2005**, *44*, 3275−3279.

(3) Shamay, E. S.; Buch, V.; Parrinello, M.; Richmond, G. L. At the water's edge: Nitric acid as a weak acid. *J. Am. Chem. Soc.* **2007**, *129*, 12910−12911.

(4) Wang, S. Z.; Bianco, R.; Hynes, J. T. Depth-Dependent Dissociation of Nitric Acid at an Aqueous Surface: Car-Parrinello Molecular Dynamics. *J. Phys. Chem. A* **2009**, *113*, 1295−1307.

(5) Baer, M. D.; Tobias, D. J.; Mundy, C. J. Investigation of Interfacial and Bulk Dissociation of HBr, HCl, and HNO₃ Using Density Functional Theory-Based Molecular Dynamics Simulations. *J. Phys. Chem. C* **2014**, *118*, 29412−29420.

(6) Mishra, H.; Enami, S.; Nielsen, R. J.; Hoffmann, M. R.; Goddard, W. A.; Colussi, A. J. Anions dramatically enhance proton transfer through aqueous interfaces. *Proc. Natl. Acad. Sci. U. S. A.* **2012**, *109*, 10228−10232.

(7) Mishra, H.; Enami, S.; Nielsen, R. J.; Stewart, L. A.; Hoffmann, M. R.; Goddard, W. A.; Colussi, A. J. Brønsted basicity of the air-water interface. *Proc. Natl. Acad. Sci. U. S. A.* **2012**, *109*, 18679−18683.

(8) Murdachaew, G.; Nathanson, G. M.; Gerber, R. B.; Halonen, L. Deprotonation of formic acid in collisions with a liquid water surface studied by molecular dynamics and metadynamics simulations. *Phys. Chem. Chem. Phys.* **2016**, *18*, 29756−29770.

(9) Schnitzer, C.; Baldelli, S.; Campbell, D.; Shultz, M. J. Sum Frequency Generation of O-H Vibrations on the Surface of H₂O/HNO₃ Solutions and Liquid HNO₃. *J. Phys. Chem. A* **1999**, *103*, 6383−6386.

(10) Donaldson, D.; Anderson, D. Does molecular HNO₃ adsorb onto sulfuric acid droplet surfaces? *Geophys. Res. Lett.* **1999**, *26*, 3625−3628.

(11) Soule, M. C. K.; Blower, P. G.; Richmond, G. L. Nonlinear vibrational spectroscopic studies of the adsorption and speciation of nitric acid at the vapor/acid solution interface. *J. Phys. Chem. A* **2007**, *111*, 3349−3357.

(12) Lewis, T.; Winter, B.; Stern, A. C.; Baer, M. D.; Mundy, C. J.; Tobias, D. J.; Hemminger, J. C. Does nitric acid dissociate at the aqueous solution surface? *J. Phys. Chem. C* **2011**, *115*, 21183−21190.

(13) Lewis, T.; Winter, B.; Stern, A. C.; Baer, M. D.; Mundy, C. J.; Tobias, D. J.; Hemminger, J. C. Dissociation of strong acid revisited: X-ray photoelectron spectroscopy and molecular dynamics simulations of HNO₃ in water. *J. Phys. Chem. B* **2011**, *115*, 9445−9451.

(14) Yang, H.; Finlayson-Pitts, B. J. Infrared spectroscopic studies of binary solutions of nitric acid and water and ternary solutions of nitric acid, sulfuric acid, and water at room temperature: Evidence for molecular nitric acid at the surface. *J. Phys. Chem. A* **2001**, *105*, 1890−1896.

(15) Leopold, K. R. Hydrated acid clusters. *Annu. Rev. Phys. Chem.* **2011**, *62*, 327−349.

(16) Mishra, H.; Nielsen, R. J.; Enami, S.; Hoffmann, M. R.; Colussi, A. J.; Goddard III, W. A. Quantum chemical insights into the dissociation of nitric acid on the surface of aqueous electrolytes. *Int. J. Quantum Chem.* **2013**, *113*, 413−417.

(17) Kulmala, M.; Toivonen, A.; Mattila, T.; Korhonen, P. Variations of cloud droplet concentrations and the optical properties of clouds due to changing hygroscopicity: A model study. *J. Geophys. Res.-Atmos.* **1998**, *103*, 16183−16195.

(18) Seinfeld, J. H.; Pandis, S. N. *Atmospheric Chemistry and Physics: From Air Pollution to Climate Change*, 2nd ed.; Wiley: New York, 2006.

(19) Lelieveld, J.; Crutzen, P. J. The role of clouds in tropospheric photochemistry. *J. Atmos. Chem.* **1991**, *12*, 229−267.

(20) Carl, S. A.; Ingham, T.; Moortgat, G. K.; Crowley, J. N. OH kinetics and photochemistry of HNO₃ in the presence of water vapor. *Chem. Phys. Lett.* **2001**, *341*, 93−98.

(21) Dulitz, K.; Amedro, D.; Dillon, T. J.; Pozzer, A.; Crowley, J. N. Temperature-(208−318 K) and pressure-(18−696Torr) dependent rate coefficients for the reaction between OH and HNO₃. *Atmos. Chem. Phys.* **2018**, *18*, 2381−2394.

(22) Staikova, M.; Donaldson, D. Ab initio investigation of water complexes of some atmospherically important acids: HONO, HNO₃ and HO₂ NO₂. *Phys. Chem. Chem. Phys.* **2001**, *3*, 1999−2006.

(23) Gonzalez, J.; Anglada, J. M. Gas phase reaction of nitric acid with hydroxyl radical without and with water. A theoretical investigation. *J. Phys. Chem. A* **2010**, *114*, 9151−9162.

(24) Finlayson-Pitts, B. J.; Wingen, L. M.; Sumner, A. L.; Syomin, D.; Ramazan, K. A. The heterogeneous hydrolysis of NO₂ in laboratory systems and in outdoor and indoor atmospheres: An integrated mechanism. *Phys. Chem. Chem. Phys.* **2003**, *5*, 223−242.

(25) Dubowski, Y.; Sumner, A. L.; Menke, E.; Gaspar, D. J.; Newberg, J.; Hoffman, R. C.; Penner, R.; Hemminger, J.; Finlayson-Pitts, B. J. Interactions of gaseous nitric acid with surfaces of environmental interest. *Phys. Chem. Chem. Phys.* **2004**, *6*, 3879−3888.

(26) Ramazan, K.; Wingen, L. M.; Miller, Y.; Chaban, G. M.; Gerber, R. B.; Xantheas, S. S.; Finlayson-Pitts, B. J. New experimental and theoretical approach to the heterogeneous hydrolysis of NO₂: key role of molecular nitric acid and its complexes. *J. Phys. Chem. A* **2006**, *110*, 6886−6897.

(27) Knipping, E. M.; Dabdub, D. Modeling surface-mediated renoxification of the atmosphere via reaction of gaseous nitric oxide with deposited nitric acid. *Atmos. Environ.* **2002**, *36*, 5741−5748.

(28) Rivera-Figueroa, A. M.; Sumner, A. L.; Finlayson-Pitts, B. J. Laboratory Studies of Potential Mechanisms of Renoxification of Tropospheric Nitric Acid. *Environ. Sci. Technol.* **2003**, *37*, 548−554.

(29) Handley, S. R.; Clifford, D.; Donaldson, D. Photochemical loss of nitric acid on organic films: A possible recycling mechanism for NOₓ. *Environ. Sci. Technol.* **2007**, *41*, 3898−3903.

(30) Finlayson-Pitts, B. J. Reactions at surfaces in the atmosphere: integration of experiments and theory as necessary (but not necessarily sufficient) for predicting the physical chemistry of aerosols. *Phys. Chem. Chem. Phys.* **2009**, *11*, 7760−7779.

(31) Zhou, X.; Zhang, N.; TerAvest, M.; Tang, D.; Hou, J.; Bertman, S.; Alaghmand, M.; Shepson, P. B.; Carroll, M. A.; Griffith, S.; et al. Nitric acid photolysis on forest canopy surface as a source for tropospheric nitrous acid. *Nat. Geosci.* **2011**, *4*, 440−443.

(32) Baergen, A. M.; Donaldson, D. Photochemical renoxification of nitric acid on real urban grime. *Environ. Sci. Technol.* **2013**, *47*, 815−820.

(33) Ye, C.; Gao, H.; Zhang, N.; Zhou, X. Photolysis of nitric acid and nitrate on natural and artificial surfaces. *Environ. Sci. Technol.* **2016**, *50*, 3530−3536.

(34) Zhou, X.; Gao, H.; He, Y.; Huang, G.; Bertman, S. B.; Civerolo, K.; Schwab, J. Nitric acid photolysis on surfaces in low-NOₓ environments: Significant atmospheric implications. *Geophys. Res. Lett.* **2003**, *30*, 018620.

(35) Schuttlefield, J.; Rubasinghege, G.; El-Maazawi, M.; Bone, J.; Grassian, V. H. Photochemistry of adsorbed nitrate. *J. Am. Chem. Soc.* **2008**, *130*, 12210−12211.

(36) Zhu, C.; Xiang, B.; Chu, L. T.; Zhu, L. 308 nm photolysis of nitric acid in the gas phase, on aluminum surfaces, and on ice films. *J. Phys. Chem. A* **2010**, *114*, 2561−2568.

(37) Saliba, N.; Yang, H.; Finlayson-Pitts, B. Reaction of gaseous nitric oxide with nitric acid on silica surfaces in the presence of water at room temperature. *J. Phys. Chem. A* **2001**, *105*, 10339−10346.

(38) Chen, H.; Navea, J. G.; Young, M. A.; Grassian, V. H. Heterogeneous photochemistry of trace atmospheric gases with

components of mineral dust aerosol. *J. Phys. Chem. A* **2011**, *115*, 490−499.

(39) Ye, C.; Zhang, N.; Gao, H.; Zhou, X. Matrix effect on surface-catalyzed photolysis of nitric acid. *Sci. Rep.* **2019**, *9*, 4351.

(40) Bianco, R.; Wang, S.; Hynes, J. T. Theoretical study of the dissociation of nitric acid at a model aqueous surface. *J. Phys. Chem. A* **2007**, *111*, 11033−11042.

(41) Wang, S.; Bianco, R.; Hynes, J. T. Nitric Acid Dissociation at an Aqueous Surface: Occurrence and Mechanism. *Isr. J. Chem.* **2009**, *49*, 251−259.

(42) Wang, S.; Bianco, R.; Hynes, J. T. An atmospherically relevant acid: $HNO_3$. *Comput. Theor. Chem.* **2011**, *965*, 340−345.

(43) Field, M. J.; Bash, P. A.; Karplus, M. A combined quantum mechanical and molecular mechanical potential for molecular dynamics simulations. *J. Comput. Chem.* **1990**, *11*, 700−733.

(44) Becke, A. D. Density-Functional thermochemistry. iii. The role of exact exchange. *J. Chem. Phys.* **1993**, *98*, 5648−5652.

(45) Hehre, W. J.; Ditchfield, R.; Pople, J. A. Self—Consistent Molecular Orbital Methods. XII. Further Extensions of Gaussian—Type Basis Sets for Use in Molecular Orbital Studies of Organic Molecules. *J. Chem. Phys.* **1972**, *56*, 2257−2261.

(46) Hehre, W. J.; Stewart, R. F.; Pople, J. A. Self-consistent molecular orbital methods. I Use of gaussian expansions of Slater-type atomic orbitals. *J. Chem. Phys.* **1969**, *51*, 2657−2664.

(47) Krishnan, R.; Binkley, J. S.; Seeger, R.; Pople, J. A. Self-Consistent Molecular-Orbital Methods. 20. Basis Set For Correlated Wave-Functions. *J. Chem. Phys.* **1980**, *72*, 650−654.

(48) Jorgensen, W. L.; Chandrasekhar, J.; Madura, J. D.; Impey, R. W.; Klein, M. L. Comparison of simple potential functions for simulating liquid water. *J. Chem. Phys.* **1983**, *79*, 926−935.

(49) Dang, L. X.; Pettitt, B. M. Simple intramolecular model potentials for water. *J. Phys. Chem.* **1987**, *91*, 3349−3354.

(50) Jorgensen, W. L.; Tirado-Rives, J. The OPLS potential functions for proteins, energy minimizations for crystals of cyclic peptides and crambin. *J. Am. Chem. Soc.* **1988**, *110*, 1657−1666.

(51) Martins-Costa, M. T. C.; Anglada, J. M.; Francisco, J. S.; Ruiz-Lopez, M. Reactivity of Atmospherically Relevant Small Radicals at the Air-Water Interface. *Angew. Chem., Int. Ed.* **2012**, *51*, 5413−5417.

(52) Martins-Costa, M. T. C.; Anglada, J. M.; Francisco, J. S.; Ruiz-Lopez, M. F. Reactivity of Volatile Organic Compounds at the Surface of a Water Droplet. *J. Am. Chem. Soc.* **2012**, *134*, 11821−11827.

(53) Anglada, J. M.; Martins-Costa, M. T. C.; Ruiz-Lopez, M. F.; Francisco, J. S. Spectroscopic signatures of ozone at the air-water interface and photochemistry implications. *Proc. Natl. Acad. Sci. U. S. A.* **2014**, *111*, 11618−11623.

(54) Anglada, J. M.; Martins-Costa, M.; Francisco, J. S.; Ruiz-Lopez, M. F. Interconnection of Reactive Oxygen Species Chemistry across the Interfaces of Atmospheric, Environmental, and Biological Processes. *Acc. Chem. Res.* **2015**, *48*, 575−583.

(55) Martins-Costa, M. T. C.; Garcia-Prieto, F. F.; Ruiz-Lopez, M. F. Reactivity of aldehydes at the air-water interface. Insights from molecular dynamics simulations and ab initio calculations. *Org. Biomol. Chem.* **2015**, *13*, 1673−1679.

(56) Martins-Costa, M. T. C.; Anglada, J. M.; Francisco, J. S.; Ruiz-López, M. F. Impacts of cloud water droplets on the OH production rate from peroxide photolysis. *Phys. Chem. Chem. Phys.* **2017**, *19*, 31621−31627.

(57) Martins-Costa, M. T. C.; Ruiz-López, M. F. Highly accurate computation of free energies in complex systems through horsetail QM/MM molecular dynamics combined with free-energy perturbation theory. *Theor. Chem. Acc.* **2017**, *136*, 50.

(58) Martins-Costa, M. T. C.; Ruiz-López, M. F. Reaching multi-nanosecond timescales in combined QM/MM molecular dynamics simulations through parallel horsetail sampling. *J. Comput. Chem.* **2017**, *38*, 659−668.

(59) Bistafa, C.; Kitamura, Y.; Martins-Costa, M. T. C.; Nagaoka, M.; Ruiz-López, M. F. A Cost-Effective Method for Free-Energy Minimization in Complex Systems with Elaborated Ab Initio Potentials. *J. Chem. Theory Comput.* **2018**, *14*, 3262−3271.

(60) Hoover, W. G. Canonical dynamics: Equilibrium phase-space distributions. *Phys. Rev. A: At., Mol., Opt. Phys.* **1985**, *31*, 1695−1697.

(61) Nosé, S. A unified formulation of the constant temperature molecular dynamics methods. *J. Chem. Phys.* **1984**, *81*, 511−519.

(62) Martins-Costa, M. T. C.; Ruiz-López, M. F. Molecular dynamics of hydrogen peroxide in liquid water using a combined quantum/classical force field. *Chem. Phys.* **2007**, *332*, 341−347.

(63) Frisch, M. J.; Trucks, G. W.; Schlegel, H. B.; Scuseria, G. E.; Robb, M. A.; Cheeseman, J. R.; Scalmani, G.; Barone, V.; Mennucci, B.; Petersson, G. A.; et al. *Gaussian 09*; Gaussian, Inc.: Wallingford, CT, 2009.

(64) Ponder, J. W. *TINKER: Software Tools for Molecular Design 4.2*; Washington University School of Medicine: Saint Louis, MO, 2004.

(65) Marian, C. M.; Heil, A.; Kleinschmidt, M. The DFT/MRCI method. *Wiley Interdiscip. Rev.: Comput. Mol. Sci.* **2019**, *9*, No. e1394.

(66) Neese, F. The ORCA program system. *Wiley Interdiscip. Rev.: Comput. Mol. Sci.* **2012**, *2*, 73−78.

(67) Weigend, F.; Ahlrichs, R. Balanced basis sets of split valence, triple zeta valence and quadruple zeta valence quality for H to Rn: Design and assessment of accuracy. *Phys. Chem. Chem. Phys.* **2005**, *7*, 3297−3305.

(68) Hellweg, A.; Rappoport, D. Development of new auxiliary basis functions of the Karlsruhe segmented contracted basis sets including diffuse basis functions (def2-SVPD, def2-TZVPPD, and def2-QVPPD) for RI-MP2 and RI-CC calculations. *Phys. Chem. Chem. Phys.* **2015**, *17*, 1010−1017.

(69) Torrent-Sucarrat, M.; Ruiz-Lopez, M. F.; Martins-Costa, M.; Francisco, J. S.; Anglada, J. M. Protonation of water clusters induced by hydroperoxyl radical surface adsorption. *Chem. - Eur. J.* **2011**, *17*, 5076−5085.

(70) Ruiz-Lopez, M. F.; Martins-Costa, M. T.; Anglada, J. M.; Francisco, J. S. A New Mechanism of Acid Rain Generation from HOSO at the Air-Water Interface. *J. Am. Chem. Soc.* **2019**, *141*, 16564−16568.

(71) Martins-Costa, M. T. C.; Ruiz-López, M. F. Isoprene Reactivity on Water Surfaces from ab initio QM/MM Molecular Dynamics Simulations. *ChemPhysChem* **2020**, *21*, 2263−2271.

(72) Frisch, M. J.; Pople, J. A.; Binkley, J. S. Self-Consistent Molecular Orbital Methods 25: Supplementary Functions for Gaussian Basis Sets. *J. Chem. Phys.* **1984**, *80*, 3265−3269.

(73) Hehre, W. J.; Radom, L.; Schleyer, P. v. R.; Pople, J. A. *Ab Initio Molecular Orbital Theory*; Wiley: New York, 1986.

(74) McLean, A.; Lengsfield III, B.; Pacansky, J.; Ellinger, Y. Symmetry breaking in molecular calculations and the reliable prediction of equilibrium geometries. The formyloxyl radical as an example. *J. Chem. Phys.* **1985**, *83*, 3567−3576.

(75) Zhang, I. Y.; Wu, J.; Xu, X. Extending the reliability and applicability of B3LYP. *Chem. Commun.* **2010**, *46*, 3057−3070.

(76) Liakos, D. G.; Guo, Y.; Neese, F. Comprehensive Benchmark Results for the Domain Based Local Pair Natural Orbital Coupled Cluster Method (DLPNO-CCSD (T)) for Closed-and Open-Shell Systems. *J. Phys. Chem. A* **2020**, *124*, 90−100.

(77) Dunning, T. H. J. Gaussian Basis Sets for Use in Correlated Molecular Calculations. I. The Atoms Boron through Neon and Hydrogen. *J. Chem. Phys.* **1989**, *90*, 1007−1023.

(78) Kendall, R. A.; Dunning, T. H.; Harrison, R. J. Electron affinities of the first-row atoms revisited. Systematic basis sets and wave functions. *J. Chem. Phys.* **1992**, *96*, 6796−6806.

(79) Lee, Y. S.; Kucharski, S. A.; Bartlett, R. J. A coupled cluster approach with triple excitations. *J. Chem. Phys.* **1984**, *81*, 5906−5912.

(80) Bak, K. L.; Gauss, J.; Jørgensen, P.; Olsen, J.; Helgaker, T.; Stanton, J. F. The accurate determination of molecular equilibrium structures. *J. Chem. Phys.* **2001**, *114*, 6548−6556.

(81) Lu, D. H.; Truong, T. N.; Melissas, V. S.; Lynch, G. C.; Liu, Y.-P.; Garrett, B. C.; Steckler, R.; Isaacson, A. D.; Rai, S. N.; Hancock, G. C.; et al. POLYRATE-version 4.0.1. *Comput. Phys. Commun.* **1992**, *71*, 235−262.

(82) McCurdy, P. R.; Hess, W. P.; Xantheas, S. S. Nitric Acid- Water Complexes: Theoretical Calculations and Comparison to Experiment. *J. Phys. Chem. A* **2002**, *106*, 7628−7635.

(83) Escribano, R.; Couceiro, M.; Gómez, P.; Carrasco, E.; Moreno, M.; Herrero, V. The nitric acid hydrates: Ab initio molecular study, and RAIR spectra of the solids. *J. Phys. Chem. A* **2003**, *107*, 651−661.

(84) Reed, A. E.; Curtiss, L. A.; Weinhold, F. Intermolecular interactions from a natural bond orbital, donor-acceptor viewpoint. *Chem. Rev.* **1988**, *88*, 899−926.

(85) Minofar, B.; Vácha, R.; Wahab, A.; Mahiuddin, S.; Kunz, W.; Jungwirth, P. Propensity for the air/water interface and ion pairing in magnesium acetate vs magnesium nitrate solutions: Molecular dynamics simulations and surface tension measurements. *J. Phys. Chem. B* **2006**, *110*, 15939−15944.

(86) Dang, L. X.; Chang, T.-M.; Roeselova, M.; Garrett, B. C.; Tobias, D. J. On $NO_3^-$-$H_2O$ interactions in aqueous solutions and at interfaces. *J. Chem. Phys.* **2006**, *124*, 066101.

(87) Thomas, J. L.; Roeselova, M.; Dang, L. X.; Tobias, D. J. Molecular dynamics simulations of the solution- air interface of aqueous sodium nitrate. *J. Phys. Chem. A* **2007**, *111*, 3091−3098.

(88) Miller, Y.; Thomas, J. L.; Kemp, D. D.; Finlayson-Pitts, B. J.; Gordon, M. S.; Tobias, D. J.; Gerber, R. B. Structure of large nitrate-water clusters at ambient temperatures: simulations with effective fragment potentials and force fields with implications for atmospheric chemistry. *J. Phys. Chem. A* **2009**, *113*, 12805−12814.

(89) Otten, D. E.; Petersen, P. B.; Saykally, R. J. Observation of nitrate ions at the air/water interface by UV-second harmonic generation. *Chem. Phys. Lett.* **2007**, *449*, 261−265.

(90) Brown, M. A.; Winter, B.; Faubel, M.; Hemminger, J. C. Spatial distribution of nitrate and nitrite anions at the liquid/vapor interface of aqueous solutions. *J. Am. Chem. Soc.* **2009**, *131*, 8354−8355.

(91) Tobias, D. J.; Stern, A. C.; Baer, M. D.; Levin, Y.; Mundy, C. J. Simulation and Theory of Ions at Atmospherically Relevant Aqueous Liquid-Air Interfaces. *Annu. Rev. Phys. Chem.* **2013**, *64*, 339−359.

(92) Burkholder, J.; Sander, S.; Abbatt, J.; Barker, J.; Huie, R.; Kolb, C.; Kurylo, M.; Orkin, V.; Wilmouth, D.; Wine, P. *Chemical kinetics and photochemical data for use in atmospheric studies*, evaluation no. 18; Jet Propulsion Laboratory, National Aeronautics and Space Administration: Pasadena, CA, 2015.

(93) Warneck, P.; Williams, J. *The Atmospheric Chemist's Companion. Numerical Data for Use in the Atmospheric Sciences*; Springer: Netherlands, 2012.

(94) Finlayson-Pitts, B. J.; Pitts, J. N., Jr. *Atmospheric Chemistry: Fundamental and Experimental Techniques*; Wiley: New York, 1986.

(95) Riffault, V.; Gierczak, T.; Burkholder, J. B.; Ravishankara, A. R. Quantum yields for OH production in the photodissociation of $HNO_3$ at 248 and 308 nm and $H_2O_2$ at 308 and 320 nm. *Phys. Chem. Chem. Phys.* **2006**, *8*, 1079−1085.

(96) Zhu, L.; Sangwan, M.; Huang, L.; Du, J.; Chu, L. T. Photolysis of Nitric Acid at 308 nm in the Absence and in the Presence of Water Vapor. *J. Phys. Chem. A* **2015**, *119*, 4907−4914.

(97) Nissenson, P.; Knox, C. J.; Finlayson-Pitts, B. J.; Phillips, L. F.; Dabdub, D. Enhanced photolysis in aerosols: evidence for important surface effects. *Phys. Chem. Chem. Phys.* **2006**, *8*, 4700−4710.

(98) Anglada, J. M.; Crehuet, R.; Solé, A. The gas phase oxidation of HCOOH by Cl and $NH_2$ radicals. Proton coupled electron transfer versus hydrogen atom transfer. *Mol. Phys.* **2019**, *117*, 1430−1441.

(99) Anglada, J. M.; Sole, A. The atmospheric oxidation of HONO by OH, Cl, and ClO radicals. *J. Phys. Chem. A* **2017**, *121*, 9698−9707.

(100) Anglada, J. M.; Olivella, S.; Solé, A. Unexpected reactivity of amidogen radical in the gas phase degradation of nitric acid. *J. Am. Chem. Soc.* **2014**, *136*, 6834−6837.

(101) Anglada, J. M.; Olivella, S.; Solé, A. Atmospheric formation of the $NO_3$ radical from gas-phase reaction of $HNO_3$ acid with the $NH_2$ radical: Proton-coupled electron-transfer versus hydrogen atom transfer mechanisms. *Phys. Chem. Chem. Phys.* **2014**, *16*, 19437−19445.

(102) Anglada, J. M.; Olivella, S.; Solé, A. Hydrogen transfer between sulfuric acid and hydroxyl radical in the gas phase:

(103) Anglada, J. M.; Gonzalez, J. Different catalytic effects of a single water molecule: the gas-phase reaction of formic acid with hydroxyl radical in water vapor. *ChemPhysChem* **2009**, *10*, 3034−3045.

(104) Olivella, S.; Anglada, J. M.; Solé, A.; Bofill, J. M. Mechanism of the hydrogen transfer from the OH group to oxygen-centered radicals: proton-coupled electron-transfer versus radical hydrogen abstraction. *Chem. - Eur. J.* **2004**, *10*, 3404−3410.

(105) Anglada, J. M.; Martins-Costa, M. T. C.; Francisco, J. S.; Ruiz-López, M. F. Triplet state promoted reaction of $SO_2$ with $H_2O$ by competition between proton coupled electron transfer (pcet) and hydrogen atom transfer (hat) processes. *Phys. Chem. Chem. Phys.* **2019**, *21*, 9779−9784.

(106) Anglada, J. M. Complex mechanism of the gas phase reaction between formic acid and hydroxyl radical. Proton coupled electron transfer versus radical hydrogen abstraction mechanisms. *J. Am. Chem. Soc.* **2004**, *126*, 9809−9820.

(107) Brown, S. S.; Talukdar, R. K.; Ravishankara, A. Reconsideration of the rate constant for the reaction of hydroxyl radicals with nitric acid. *J. Phys. Chem. A* **1999**, *103*, 3031−3037.

(108) Huang, T.; Li, Z.; Ma, B.; Long, Y. Tracing the Origin of Groundwater Nitrate in an Area Affected by Acid Rain Using Dual Isotopic Composition of Nitrate. *Geofluids* **2019**, *2019*, 8964182.

(109) Barth, M.; Sillman, S.; Hudman, R.; Jacobson, M.; Kim, C. H.; Monod, A.; Liang, J. Summary of the cloud chemistry modeling intercomparison: Photochemical box model simulation. *J. Geophys. Res.* **2003**, *108*, 002673.

(110) Paulson, S. E.; Gallimore, P. J.; Kuang, X. B. M.; Chen, J. R.; Kalberer, M.; Gonzalez, D. H. A light-driven burst of hydroxyl radicals dominates oxidation chemistry in newly activated cloud droplets. *Sci. Adv.* **2019**, *5*, No. eaav7689.

(111) Kameel, F. R.; Hoffmann, M.; Colussi, A. OH radical-initiated chemistry of isoprene in aqueous media. Atmospheric implications. *J. Phys. Chem. A* **2013**, *117*, 5117−5123.

(112) Vácha, R.; Slavíček, P.; Mucha, M.; Finlayson-Pitts, B. J.; Jungwirth, P. Adsorption of Atmospherically relevant Gases at the Air/Water Interface: Free Energy Profiles of Aqueous Solvation of $N_2$, $O_2$, $O_3$, OH, $H_2O$, $HO_2$, and $H_2O_2$. *J. Phys. Chem. A* **2004**, *108*, 11573−11579.

(113) Li, S.; Liu, W.; Xie, P.; Li, A.; Qin, M.; Peng, F.; Zhu, Y. Observation of the nighttime nitrate radical in Hefei, China. *J. Environ. Sci. (Beijing, China)* **2008**, *20*, 45−49.

(114) Brown, S. S.; Stutz, J. Nighttime radical observations and chemistry. *Chem. Soc. Rev.* **2012**, *41*, 6405−6447.

(115) Sander, R. Compilation of Henry's law constants (version 4.0) for water as solvent. *Atmos. Chem. Phys.* **2015**, *15*, 4399−4981.

(116) Mezyk, S. P.; Cullen, T. D.; Rickman, K. A.; Mincher, B. J. The reactivity of the nitrate radical ($^\bullet NO_3$) in aqueous and organic solutions. *Int. J. Chem. Kinet.* **2017**, *49*, 635−642.

Competition among hydrogen atom transfer, proton-coupled electron-transfer, and double proton transfer. *J. Phys. Chem. A* **2006**, *110*, 1982−1990.